Shaping for PET image analysis

Eloïse Grossiord, Nicolas Passat, Hugues Talbot, Benoît Naegel, Salim Kanoun, Ilan Tal, Pierre Tervé, Soléakhéna Ken, Olivier Casasnovas, Michel Meignan, et al.

Shaping for PET image analysis

Éloïse Grossiord[a,b], Nicolas Passat[c], Hugues Talbot[d], Benoît Naegel[e], Salim Kanoun[f], Ilan Tal[g], Pierre Tervé[h], Soléakhéna Ken[b], Olivier Casasnovas[i], Michel Meignan[j], Laurent Najman[k]

[a]*Institut de Mathématiques de Toulouse; UMR5219; Université de Toulouse; CNRS UPS IMT F-31062 Toulouse CEDEX 9, France*
[b]*Institut Universitaire du Cancer Toulouse Oncopôle (IUCT-O) - Institut Claudius Regaud; Département d'Ingénierie et de Physique Médicale, F-31059 Toulouse CEDEX 9, France*
[c]*Université de Reims Champagne Ardenne, CReSTIC EA 3804, 51097 Reims, France*
[d]*CentraleSupélec, INRIA GALEN team, Université Paris-Saclay, France*
[e]*ICube, Université de Strasbourg, CNRS, France*
[f]*Institut Universitaire du Cancer Toulouse Oncopôle (IUCT-O) - Institut Claudius Regaud; Département d'Imagerie Médicale, F-31059 Toulouse CEDEX 9, France*
[g]*Haifa, Israel*
[h]*Keosys Medical Imaging, Nantes, France*
[i]*Hematology, CHU Dijon, Dijon, France*
[j]*The Lymphoma Academic Research Organisation (LYSARC), Lyon, France*
[k]*Université Paris-Est, ESIEE-Paris, LIGM, CNRS, France*

Abstract

Component-trees constitute an efficient data structure for hierarchical image modeling. In particular they are relevant for processing and analyzing images where the structures of interest correspond either to local maxima or local minima of intensity. This is indeed the case of functional data in medical imaging. This motivates the use of component-tree-based approaches for analyzing Positron Emission Tomography (PET) images in the context of oncology. In this article, we present a simple, yet efficient, methodological framework for PET image analysis based on component-trees. More precisely, we show that the second-order paradigm of shaping, that broadly consists of computing the component-tree of a component-tree, provides a relevant way of generalizing the threshold-based strategies classically used by medical practitioners for handling PET images. In addition, it also allows to embed relevant priors regarding the sought cancer lesions.

1. Introduction

The component-tree, introduced by Salembier and et al. (1998) twenty years ago, constitutes one of the most popular hierarchical data structures for image modeling, processing and analysis. Defined and developed in the context of connected operators (Salembier and Wilkinson, 2009) —a subdomain of mathematical morphology— the component-tree allows one to model, in a lossless way, any grey-level image, based on the representation of the inclusion hierarchy of connected components obtained at the successive level sets of the image.

Its successful involvement in various application fields mainly relies on its computational efficiency. Indeed, on the one hand, the component-tree can be constructed in (quasi-)linear time. Various sequential and distributed algorithms were developed for that purpose; a recent survey was proposed by Carlinet and Géraud (2014). On the other hand, the component-tree can be processed efficiently either by local attribute-based strategies (i.e. node selection, democratized by Jones (1999)) or by global optimization strategies (i.e. tree-cut computation, formalized by Guigues and et al. (2006)), leading once again to linear time costs.

On the one hand, the component-tree is designed for handling grey-level images, i.e. images where values are

organized with respect to a total ordering. In particular, it is based either on the $\leq$ or the $\geq$ order on $\mathbb{Z}$ or $\mathbb{R}$, leading to the so-called max-trees or min-trees, that emphasize regions of interest of locally maximal or locally minimal values, respectively.

On the other hand, except for the $\leq$ or $\geq$ total ordering and the chosen topological structure of the image support, the component-tree is a parameter-free data structure. This implies that the construction of the component-tree from an image deterministically leads to a unique result. This property, together with the fact that the component-tree is a lossless model (i.e. it allows for reversible, non-altering transformations from image to tree and from tree to image), opened the way to the involvement of component-trees in the design of grey-level image processing and analysis methods and tools, in particular in the context of antiextensive filtering and segmentation (Salembier and et al., 1998; Jones, 1999).

Among many other application areas, the component-tree has been involved in the field of nuclear imaging, and more specifically Positron Emission Tomography (PET). Indeed, based on its specific properties, it constitutes a relevant data structure for modeling and processing functional medical images, where the strength of the signal is correlated to the intensity of the observed physiological phenomenon. In this context, the first domain where component-trees were involved was angiographic imaging, that emphasizes the flowing blood in vascular networks. Various filtering, vessel enhancement and segmentation methods were designed based on component-trees, as proposed e.g. by Wilkinson and Westenberg (2001); Caldairou et al. (2010); Dufour et al. (2013).

Relying on the fact that high metabolic activity regions appear as hyperintense areas in PET images, methods were designed to take advantage of the mixed spatial-spectral organization of PET information in component-trees to develop classification strategies (Alvarez Padilla and et al., 2015; Grossiord and et al., 2017) or filtering / segmentation methods (Urien and et al., 2017; Alvarez Padilla and et al., 2018a,b). Indeed, PET visualizes metabolic activity characterized by the intensity of an injected radiotracer. It is routinely used in cancer imaging for diagnosis and characterization of malignant tissues, corresponding to hyperfixations of a tracer (expressing e.g. the consumption of glucose by cancerous cells). The idea is then to highlight tumours, i.e. maximal intensities in the PET images.

In this article —which is an extended and improved version of the conference paper by Grossiord and et al. (2015a)— we present a simple, yet efficient, method for carrying out PET image analysis via a component-tree-based strategy. The novelty of this approach relies on the use of the concept of shaping, recently introduced by Xu and et al. (2016). Broadly speaking, shaping consists of computing two layers of component-trees. A first component-tree aims at modeling the grey-level image, based on intensity information. A second component-tree, built upon the first one, aims at organizing the nodes of the first tree based on second-order information. Carrying out basic operations, e.g. threshold-based tree-cut, in this second tree then allows the user to easily take into account both low-level information on the image signal and higher-level information on the structures of interest. We present this paradigm in the context of PET imaging, with the purpose of proposing a threshold-based methodology for detection of cancer lesions, guided by intensity and compacity priors.

The sequel of this article is organized as follows. In Section 2, we provide a minimal set of basic notions required to make the article self-contained. In Section 3 we recall the concepts of component-tree and shaping, and we emphasize the way of unifying shaping and standard component-tree construction from an image, via the usual graph formalism. In Section 4, we describe the methodological aspects of attribute-based filtering of component-trees with shaping. In Section 5, we instantiate our framework for tackling the issue of PET image analysis, and more precisely tumoural lesion detection based on intensity and compacity attributes. In Section 6, we describe technical details, including software production and experimental works. Section 7 briefly concludes the article by emphasizing perspective works.

2. Basic notions

Let Ω be a nonempty finite set. Let $\frown$ be an adjacency (irreflexive, symmetric) relation on Ω. The set $(\Omega, \frown)$ is a (non-directed) graph. Let $X \subseteq \Omega$ be a subset of Ω. The reflexive-transitive closure of (the restriction of) $\frown$ on X induces the connectedness relation on X. It is an equivalence relation, and the set of the equivalence classes of X, called connected components, is noted $\mathcal{C}[X]$. In

the sequel, we will assume that $(\Omega, \frown)$ is connected, i.e. $C[\Omega] = \{\Omega\}$.

Let $\mathbb{V}$ be a nonempty finite set equipped with a total order relation $\leq$. A valuation V (of Ω) is a mapping $V : \Omega \to \mathbb{V}$. For any $x \in \Omega$, $V(x) \in \mathbb{V}$ is the value of x. The triple $\mathfrak{G} = (\Omega, \frown, V)$ is called a (vertex-)valued graph.

Let $X \subseteq \Omega$ and $v \in \mathbb{V}$. The thresholding function λ_v is defined by

$$\left| \begin{array}{rcccl} \lambda_v & : & \mathbb{V}^\Omega & \to & 2^\Omega \\ & & V & \mapsto & \{x \in \Omega \mid V(x) \geq v\} \end{array} \right. \quad (1)$$

In other words, it associates to any valuation V of Ω the subset of the elements of Ω with a value greater than a given threshold parameter v.

The cylinder function $C_{(X,v)}$ is defined by

$$\left| \begin{array}{rcccl} C_{(X,v)} & : & \Omega & \to & \mathbb{V} \\ & & x & \mapsto & \left\{ \begin{array}{ll} v & \text{if } x \in X \\ \bot & \text{otherwise} \end{array} \right. \end{array} \right. \quad (2)$$

where $\bot$ is the minimal value (on $\mathbb{V}$) for the elements of Ω. A valuation $V : \Omega \to \mathbb{V}$ can be decomposed into cylinder functions induced by thresholding operations and, symmetrically, V can be reconstructed by composition of these cylinder functions

$$V = \bigvee_{v \in \mathbb{V}} \bigvee_{X \in C[\lambda_v(V)]} C_{(X,v)} \quad (3)$$

where $\vee$ is the point-wise supremum on functions of $\mathbb{V}^\Omega$. In other words, the mapping V is obtained by combining, for each value v of the space $\mathbb{V}$ and each connected component X of each binary level-set, the contribution of the cylinder function $C_{(X,v)}$ defined for the connected component X at value v. All these contributions are combined via a supremum paradigm, i.e. by considering the highest values obtained pointwise.

3. Component-trees and shaping

3.1. Component-tree

The component-tree $\mathcal{T} = (\Psi, \nearrow)$ of a valued graph $(\Omega, \frown, V)$ is the Hasse diagram (i.e. the reflexive-transitive reduction) of the partially ordered set $(\Psi, \subseteq)$, where Ψ is the set of all the connected components obtained from all the successive level sets of $(\Omega, \frown, V)$, namely

$$\Psi = \bigcup_{v \in \mathbb{V}} C[\lambda_v(V)] \quad (4)$$

Each connected component / element of Ψ is called a node of the component-tree. The root of the component-tree, namely Ω is the unique connected component of $\lambda_\bot(V)$; it is the maximum of $(\Psi, \subseteq)$. The leaves of the component-tree are all the nodes which are minimal elements of $(\Psi, \subseteq)$.

For two nodes $N_1, N_2 \in \Psi$, we have $N_1 \nearrow N_2$ iff $N_1 \subseteq N_2$, and there is no $N_3 \in \Psi$ such that $N_1 \subset N_3 \subset N_2$. In such case, we say that N_1 is a child node of N_2 and that N_2 is the parent node of N_1 (such parent node is unique, by definition). The root is the only node without parent node. The leaves are the only nodes without children nodes.

3.2. Component-tree of a grey-level image

A grey-level image $\Im$ is composed of a finite set of points, e.g. pixels in 2D, voxels in 3D. We note Γ this set of points.

The points of Γ are generally organized with respect to a neighbourhood relation, for instance the $2n$- or $(3^n - 1)$-adjacencies classically defined in digital topology. Such relation is indeed an adjacency relation, and is noted $\frown_\Gamma$. Two points $x, y \in \Gamma$ are neighbours if we have $x \frown_\Gamma y$.

For each point $x \in \Gamma$, the image provides a specific grey-level value within a finite set $\mathbb{K} = [\![\bot, \top]\!]$ with $\top$ the maximal value for the elements of Γ (without loss of generality, we can assume $\mathbb{K} \subset \mathbb{Z}$). For each point $x \in \Gamma$, we note $I(x)$ this value; in other words we have $I : \Gamma \to \mathbb{K}$.

Based on these facts, the image can be modeled as a triple $\Im = (\Gamma, \frown_\Gamma, I)$, i.e. as a valued graph (see Section 2). As a consequence, we can relevantly build the component-tree $\mathcal{T}_\Im$ of this image.

Basically, building a component-tree, namely either a max-tree or a min-tree, depending on the order $\leq$ or $\geq$ chosen on the grey-level values, consists of (1) building the binary connected components of the image and (2) organizing these connected components from the greatest (i.e. the root) to the lowest (i.e. the leaves) according to the standard inclusion relation $\subseteq$. In the case of a max-tree (resp. min-tree), the root corresponds to the

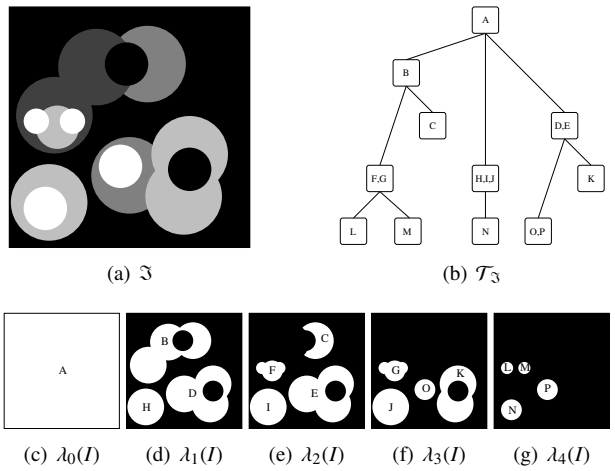

(a) $\Im$ (b) $\mathcal{T}_\Im$

(c) $\lambda_0(I)$ (d) $\lambda_1(I)$ (e) $\lambda_2(I)$ (f) $\lambda_3(I)$ (g) $\lambda_4(I)$

Figure 1: (a) A grey-level image $\Im$ defined on a square subset of $\Gamma \subset \mathbb{Z}^2$. Each point $x \in \Gamma$ has a value $I(x)$ and is equipped with the standard 4-adjacency as neighbourhood relation $\frown_\Gamma$. The values of the points of the image are within the set $\mathbb{K} = [\![0, 4]\!] \subset \mathbb{Z}$ (from 0 in black; to 4 in white). (c–g) The level sets $\lambda_v(I)$ (in white) for v varying from 0 to 4. (b) The component-tree $\mathcal{T}$ associated to I. The letters (A–P) in nodes correspond to the associated connected components (c–g).

whole support Γ, obtained by a thresholding at the lowest (resp. greatest) value, whereas the leaves are antagonistically obtained at the local maxima (resp. local minima) of the image. Building these connected components and ordering them in a hierarchical way can be considered via various paradigms, for instance by flooding or Tarjan union-find. A discussion on such construction is out of the scope of this article, and the reader is refered to (Carlinet and Géraud, 2014) for a comprehensive survey.

An example of component-tree for a grey-level image is given in Figure 1.

3.3. Shaping: component-tree of a component-tree

A component-tree $\mathcal{T} = (\Psi, \nearrow)$ is a data structure where the nodes / connected components of Ψ are hierarchically organized by $\nearrow$ with respect to the value of their level sets, from the lowest value (at the root of the component-tree) to the highest values (at the leaves of the component-tree). In other words, the component-tree expresses a value space in a spatial fashion.

A usual way to take advantage of a component-tree consists of endowing each node $N \in \Psi$ by an attribute $A(N)$, generally defined as a scalar valuation. For instance, a very classical attribute is the size of the nodes, i.e. their number of points $A(N) = |N|$. Once such attribute, namely a mapping $A : \Psi \to \mathbb{V}$ (with $\mathbb{V}$ being any set isomorphic to a part of $\mathbb{Z}$) has been defined, it is possible to perform node selection, i.e. to carry out filtering-based operations.

Endowing a component-tree $\mathcal{T} = (\Psi, \nearrow)$ with a valuation $A : \Psi \to \mathbb{V}$ is equivalent to defining a valued graph $\mathfrak{T} = (\Psi, \nearrow, A)$. (In such a case, the non-symmetric relation $\nearrow$ is considered, without loss of generality, as a symmetric one.) From such valued graph, it is in then possible to build its own component-tree; this constitutes the very paradigm of shaping.

Less formally, carrying out shaping consists of building the component-tree of a component-tree. In general, the first component-tree is built from a grey-level image (i.e. with a spectral valuation) whereas the second is built by considering an attribute on the nodes of the first (i.e. with a semantic valuation). The second component-tree then gathers, in a same data-structure, various kind of spatial (nodes), spectral (first valuation) and semantic (second valuation) information.

In particular, it is then possible to develop filtering procedures on such component-trees.

4. Attribute-based filtering with shaping – Methodology

4.1. The antiextensive filtering scheme

Let $\Im = (\Gamma, \frown_\Gamma, I)$ be a grey-level image. As evoked in Section 2, this image $\Im$ can be expressed as the supremum of the nodes of its associated component-tree $\mathcal{T}_\Im$. More precisely, Equation (3) can be rewritten as

$$I = \bigvee_{K \in \Psi} C_{(K, v_K)} \tag{5}$$

where $v_K = \max\{v \in \mathbb{V} \mid K \in C[\lambda(I)]\}$ is the maximal value that defines K as a connected component of the corresponding level set of the image. In particular, Equation (5) can be seen as a simplified version of Equation (3), where only the connected components K which are sufficiently large and with a sufficiently high value for contributing to the definition of the image I are considered (the other ones are indeed "hidden" below these large /

intense components, and then useless for defining the image).

Equation (5) leads to a well-defined image from Ψ, but also from any subset of Ψ nodes. For image processing purposes, it is possible to filter the image $\mathfrak{I}$ by discarding some of the nodes, and then reconstructing a resulting image from the subset of preserved nodes. Each point $x \in \Gamma$ in the filtered image then presents a value that is lower or equal to the initial image; the induced operators are antiextensive.

This antiextensive filtering paradigm was formalized by Salembier and et al. (1998); Jones (1999). It is basically composed of three successive steps, also illustrated in Diagram (6) :

(i) construction of the component-tree $\mathcal{T}$ associated to $\mathfrak{I}$;
(ii) reduction of Ψ, leading to a reduced component-tree $\widehat{\mathcal{T}}$; and
(iii) reconstruction of a filtered image $\widehat{\mathfrak{I}}$ induced by $\widehat{\mathcal{T}}$.

$$\begin{array}{ccc} \mathfrak{I} & \xrightarrow{(i)} & \mathcal{T} \\ \downarrow & & \downarrow (ii) \\ \widehat{\mathfrak{I}} \leq \mathfrak{I} & \xleftarrow{(iii)} & \widehat{\mathcal{T}} \end{array} \tag{6}$$

4.2. Attribute-based node selection

By assuming that each node $N \in \Psi$ is equipped with a relevant attribute value $A(N) \in \mathbb{K}$, the choice to preserve or discard N depends on a Boolean predicate $\rho : \mathbb{K} \to \{\text{true, false}\}$ acting on the attribute values.

When these attribute values are monotonic along the tree (i.e., $\rho(N)$ is true for a given node N implies the same for all the nodes between N and the root), they can be handled similarly to the grey-level of the nodes, in the sense where the node selection proceeds as a simple thresholding.

However, most attributes are not monotonic, in general. For instance, this is the case for shape attributes such as elongation or compacity, or for texture descriptors. This means that the decision for a given node does not imply its validity for the remainder of the branch. This is not an issue in the context of automated processing, where the tree is fully scanned, and ad hoc pruning policies can be applied a posteriori to homogeneize the results of the different branches of the tree; see (Salembier and et al. (1998); Jones (1999)) for a discussion on this topic.

However, our purpose is to carry out threshold-based interactive segmentation from non-monotonic attributes. To tackle this issue, we can then take advantage of the shaping paradigm.

Indeed, let us suppose that we build a second component-tree $\mathcal{T}^\star = (\Psi^\star, \nearrow^\star)$ from the first component-tree $\mathcal{T} = (\Psi, \nearrow)$, i.e. from the valued graph $\mathfrak{T} = (\Psi, \nearrow, A)$. By construction, in this new tree, each node $N^\star \in \Psi^\star$ corresponds to a set of $\mathcal{T}$ nodes (connected with respect to $\nearrow$). In addition, for any two nodes $N_1^\star, N_2^\star$ such that $N_1^\star \nearrow^\star N_2^\star$, we have the following properties

$$N \in N_1^\star \Rightarrow N \in N_2^\star \tag{7}$$

and

$$\min\{A(N) \mid N \in N_1^\star\} \geq \min\{A(N) \mid N \in N_2^\star\} \tag{8}$$

In other words, the attribute A is monotonic within $\mathcal{T}^\star$, even if it is not within $\mathcal{T}$.

4.3. The shaping antiextensive filtering scheme

It is then possible to process any grey-level image in the framework initially proposed by Salembier and et al. (1998); Jones (1999), simply by performing node selection in the second component-tree $\mathcal{T}^\star$, built from the first one $\mathcal{T}$. In particular, since the attribute computed from the nodes of $\mathcal{T}$ is now monotonic in $\mathcal{T}^\star$, we can operate thresholding / pruning approaches. The overall procedure, illustrated on Diagram (9), is quasi-linear in time and space, since we only duplicate the standard component-tree anti-extensive filtering process (Diagram (6)) to non-monotonic attributes. More precisely, the cost of the construction of a component-tree is quasi-linear in time, $S \log S \simeq \kappa . S$, where S is the size of the physical support of the image and κ a quasi-constant value. Then, the cost of (i) is approximately $|\Gamma|$ whereas the cost of (i') is approximately $|\Psi|$ with $|\Psi| < |\Gamma|$ (and in general $|\Psi| \ll |\Gamma|$). The pruning step (ii) is carried out in linear time $|\Psi^\star|$, with respect to the number of nodes of $\mathcal{T}^\star$, with $|\Psi^\star| < |\Psi|$, (and in general $|\Psi^\star| \ll |\Psi|$). The reconstruction steps (iii) and (iii') are carried out point-wise, leading to computational costs $|\Psi|$ and $|\Gamma|$, linear with respect to the primitive elements of the graphs modeled by the corresponding

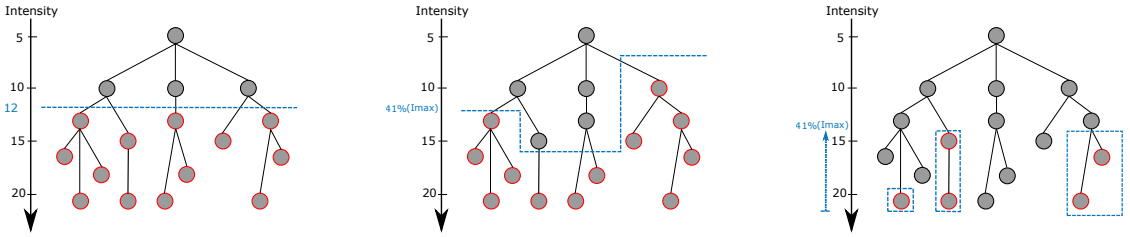

(a) Fixed (b) Adaptive (c) Bounding-box

Figure 2: The component-tree representation is compliant with all major thresholding strategies: fixed threshold (a); adaptive threshold (b); bounding-box threshold (c). Selected subsets of nodes are depicted in red.

trees. Overall, the whole computational cost is dominated by the size $|\Gamma|$ of the support of the image, due to the first and last steps of the process, leading to a quasi-linear cost with respect to the size of the image. In particular, this allows us to perform real-time threshold-based node selection.

$$\begin{array}{ccccc} \Im & \xrightarrow{(i)} & \mathcal{T} & \xrightarrow{(i')} & \mathcal{T}^\star \\ \downarrow & & & & \downarrow (ii) \\ \widehat{\Im} \leq \Im & \xleftarrow{(iii')} & \widehat{\mathcal{T}^\star} & \xleftarrow{(iii)} & \widehat{\mathcal{T}^\star} \end{array} \tag{9}$$

5. Attribute-based filtering with shaping – Application to PET image analysis

We now instantiate a PET image lesion detection framework based on the above-described methodology.

5.1. Adequacy of component-trees for PET image thresholding

As an extrema-oriented data structure, the component-tree is well adapted for emphasizing oncological lesions that correspond to maximal intensity values. In particular, the best-adapted component-tree is the max-tree, organized from the lowest to the highest values. More precisely, for a given PET image, the root of its component-tree $\mathcal{T}$ is the node Γ (i.e. the whole image support) obtained from the lowest level set, at value $\perp = 0$. Conversely, the leaves of $\mathcal{T}$ (i.e. the nodes that are minimal elements for the inclusion relation $\subseteq$) are the flat zones of the image of (locally) maximal values; they correspond to tumoural (lesions) and physiological (organs) high metabolic activity areas.

Another strength of the component-tree is that it intrinsically models the space of *all* the potential thresholding operations that can be carried out on a grey-level image. This allows for the generalized processing of all the regions of the PET image at once within the same structure. The choice of a solution within this data-structure can be performed by scanning the (decreasing) grey-level values along the branches of the tree, from its leaves to its root. In particular, this process is compliant with the major thresholding strategies:

- fixed thresholding (i.e., horizontal cut in the tree);
- adaptive thresholding (i.e., branch-specific cut in the tree);
- bounding-box thresholding (i.e., explicit choice of leaves of branches to cut in the tree).

These different strategies are illustrated in Figure 2.

Therefore, the component-tree satisfies mandatory properties for developing interactive segmentation processes in PET, in real-time thanks to its low space and time cost properties.

5.2. Shaping analysis of the component-tree based on compacity attribute

Let $\Im$ be a PET image, and let us assume that we have computed its component-tree —more precisely, its max-tree— $\mathcal{T}$ (step (i) in Diagram (9). In this tree $\mathcal{T}$, the nodes

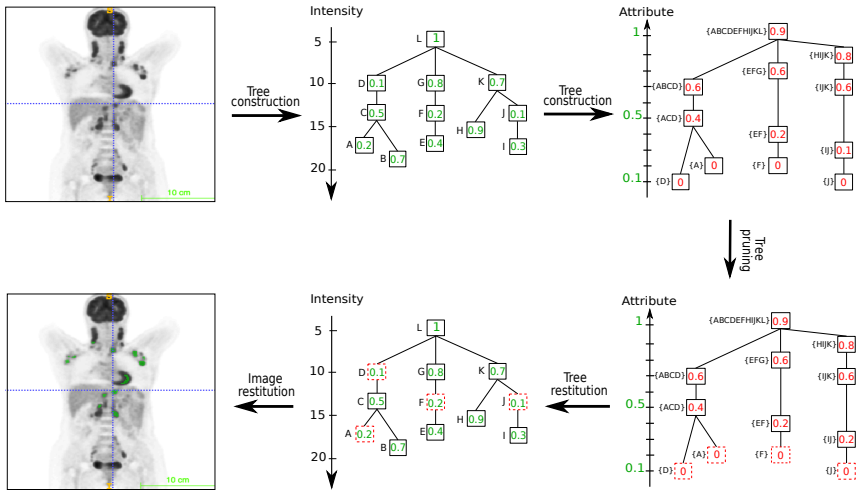

Figure 3: Illustration of the detection framework in PET, based on compacity attribute. The first component-tree $\mathcal{T}$, based on the intensity level-sets, is a max-tree. Each node N of $\mathcal{T}$ is then valued with a compacity attribute $A(N)$ (in green). The second tree $\mathcal{T}^\star$ is the min-tree of $\mathcal{T}$, based on the attribute level-sets. Each node of $\mathcal{T}^\star$ is then valued with respect to the difference between the attribute value of the leaf and that of the node (in red). The node selection is based here on a threshold of 0.1 in $\mathcal{T}^\star$ with respect to this relative attribute (discarded nodes are dashed). The remaining nodes are then propagated back from the second tree to the image support, via the first tree.

that are close to the leaves correspond to the areas of highest intensity; they can be either lesions or hyper-fixating organs.

Our purpose is to develop an interactive attribute-based procedure for identifying automatically active tumours in $\mathfrak{I}$. A segmentation strategy based only on PET value thresholding may over-segment the high intensity areas, including true positives but also many false positives. As a consequence, it is indeed required to choose and compute a relevant attribute in order to discriminate the nodes of interest within $\mathcal{T}$.

Our working hypothesis, that is in particular valid in the case of lymphoma —where the number of lesions is high and their shape is compact (similar to a sphere), compared to physiological uptakes (e.g., heart, kidneys, etc.)— is that a compacity criterion, in addition to the intensity criterion, could allow us to better discriminate the active lesions, especially in the thorax.

Consequently, we define an attribute $A : 2^\Gamma \to [0,1]$ that associates to any connected subset of Γ, a numerical value describing how the corresponding shape is compact. This attribute is computed from the eigenvalues $\lambda_1 \geq \lambda_2 \geq \lambda_3$ associated to the eigenvectors of the 3×3 matrix of inertia of the (binary) shapes $N \subseteq \Gamma$. In particular, we define

$$A(N) = \lambda_3/\lambda_1 \tag{10}$$

namely, the ratio between the lowest and highest eigenvalues, lying in $[0,1]$. If $A(N)$ is close to 1, then λ_3 and λ_1 (and thus λ_2) present similar values, and N then has a compact shape. When $A(N)$ decreases toward 0, N becomes more elongated.

This attribute A is indeed non-monotonic. In particular, it is impossible to interactively process $\mathcal{T}$ in a threshold-based fashion, based on the information carried by A. In order to tackle this issue, we rely on the shaping paradigm.

A second component-tree $\mathcal{T}^\star$ is then built from the tree $\mathcal{T} = (\Psi, \nearrow)$, i.e. from the valued graph $\mathfrak{T} = (\Psi, \nearrow, A)$ (step (i') in Diagram (9)).

Contrary to $\mathcal{T}$, that was a max-tree based on $\leq$, this second tree $\mathcal{T}^\star$ is a min-tree, based on $\geq$. Indeed, the root is the node of greatest value for A (i.e. with the highest compacity), whereas the leaves are those of locally lowest values (i.e. with the lowest compacity). The nodes that

are close to the leaves then correspond to the sets of connected components of Γ that are of least relevance, and should then be removed preferentially.

In order to segment the active lesions versus the hyperfixating organs (step (*ii*) in Diagram (9)), two distinct strategies can be considered:

- the first is an absolute thresholding along the branches of $\mathcal{T}^\star$, thus pruning the distal parts of the tree, composed of the nodes that have a compacity value A lower than a chosen threshold value $t \in [0, 1]$. This strategy enables to filter out nodes that are the least likely to be part of the expected shape, by assuming that their attribute values are in a common interval. However, it can be difficult to achieve an optimal result with a unique threshold;
- the second is a relative thresholding that considers the "gap" between the compacity value $A(N)$ of a node N and the value $A(L)$ of the leaf of its branch. This gap $A(N) - A(L)$ still varies monotonically within $[0, 1]$ along the branches, with 0 values at the leaves. This strategy consists of comparing each node with its neighbourhood in terms of shape, by taking the leaf nodes as references, namely the nodes that are the least likely to correspond to the criterion. Nodes with a shape similar to the leaf (i.e. elongated structure in this case) in each branch are associated with low difference values, and can be eliminated in that way. On the contrary, nodes corresponding to the expected shape (i.e. compact shape) are kept thanks to larger gaps in attribute values. This strategy is more flexible, since it does not require to find the optimal compacity threshold, and relies on local information. However, it can be associated with a larger variability in attribute values of preserved/eliminated nodes within the different branches, and therefore a possibly higher shape variability, compared to the absolute strategy. For instance, there is a risk of eliminating compact nodes, corresponding to branch leaves or near leaves, if there is no more elongated nodes in the branch.

In the following, the first strategy was adopted. Once the nodes of $\mathcal{T}^\star$ have been selected, the resulting image has to be computed. Each selected node $N^\star$ of $\mathcal{T}^\star$ is indeed a connected component of Ψ nodes. In order to retrieve the subset $\widehat{\Psi} \subseteq \Psi$ of selected nodes within Ψ, from the subset $\widehat{\Psi^\star} \subseteq \Psi^\star$ of selected nodes of $\mathcal{T}^\star$ (step (*iii*) in Diagram (9)), we can simply proceed by union, i.e. by setting $\widehat{\Psi} = \bigcup \widehat{\Psi^\star} = \bigcup\{\widehat{N} \in \Psi \mid \exists \widehat{N^\star} \in \widehat{\Psi^\star}, \widehat{N} \in \widehat{N^\star}\}$. In other words, a node N is preserved in $\mathcal{T}$ if it appears at least once in a preserved node $N^\star$ of $\Psi^\star$ (keeping in mind that such node N generally appears in many nodes $N^\star$).

Finally, the last step that consists of embedding the selected nodes N of $\widehat{\Psi}$ back to Γ (step (*iii'*) in Diagram (9)) can be conducted the same way: the subset $\widehat{\Gamma}$ of detected points of the image $\mathfrak{I}$ can be defined as $\widehat{\Gamma} = \bigcup \widehat{\Psi} = \bigcup\{\widehat{x} \in \Gamma \mid \exists \widehat{N} \in \widehat{\Psi}, \widehat{x} \in \widehat{N}\}$. (Note that associated grey-level information can also be retrieved by simply using Equation (5), substituting $\widehat{\Psi}$ to Ψ.)

An application of the proposed framework is exemplified in Figure 3.

6. Practical aspects

6.1. Implementation

Our proposed framework is open-source[1] and relies on the LibTIM[2] library, developed in C++ under GPL 3.0 License, which allows for the efficient construction, manipulation and processing of morphological hierarchies.

As part of the work on PET lymphoma tumour detection and segmentation, our framework has been also integrated into the Beth Israel Plugin[3] for Fiji developped by Kanoun and et al. (2016), which is a free and open-source software (also under GPL 3.0 License), plugin[4] of ImageJ that is dedicated to PET/CT (X-ray Computed Tomography) image visualization and processing. The purpose of this tool is to provide a collaborative PET/CT platform that is able to integrate research work. This software, developed in Java, is provided as a Fiji / ImageJ plugin. The viewer handles PET and CT visualization and fusion, maximum intensity projection display and a quantification tool, which now integrates the previously described shapings algorithm for detection / segmentation purpose. Our framework is integrated as a module[5], provided as an

[1] `https://github.com/egrossiord`
[2] `https://github.com/bnaegel/libtim`
[3] `https://github.com/ilan/fijiPlugins`
[4] `http://petctviewer.org`
[5] `http://petctviewer.org/index.php/feature/autosegementation`

executable called by Fiji. It takes the PET exam as an input and provides as output a segmentation mask with labeled lesions.

6.2. *Proof of concept: experiments on phantom images*

To obtain a first validation of our approach, we used the NEMA 2007 IEC image phantom. This phantom contains six spherical areas modeling lesions, with diameters 10, 13, 17, 22, 28 and 37 mm. These spheres were filled with varying ^{18}F concentrations to three different signal-to-background ratios (SBRs), namely 2.59:1, 5.06:1 and 8.40:1. Data were acquired on a Philips GEMINI TF Time-of-Flight PET/CT scanner. The PET images were obtained with the 3D LOR-RAMLA reconstruction and CT-based attenuation correction. They present a spatial resolution of 2.0 mm (Figure 4, first row).

For comparison, all images were registered to the highest contrast image. Reference segmentation was obtained by closest interactive thresholding to the known geometry on this image. The ROC curves of Figure 5 measure the set differences between the reference segmentation and our shaping result. It illustrates the impact of the signal loss on the segmentation results. The obtained results are near perfect for the image with a very high SBR of 8.40:1. In addition, even for more realistic SBRs, including that of value 2.59:1, which is low with respect to real cases, the obtained results remain satisfactory, thus underlining the relevance of the shapings approach.

6.3. *Clinical validation – Lymphoma tumour segmentation*

6.3.1. *Automated lymphoma tumour segmentation framework*

Finally, we evaluated our method in the context of lymphoma tumours detection on clinical data. The direct usage of the proposed shapings framework on PET lymphoma images, converted into SUV, leads to the automated localization / identification of lesions over the whole-body. More precisely, when lesions are homogeneous, the detected volumes match the entire lesions; however for heterogeneous ones, the most active compact regions within them are detected. Therefore, it is necessary for clinical purpose to combine this detection framework with a segmentation process to retrieve accurate tumour contours and obtain final tumour volumes.

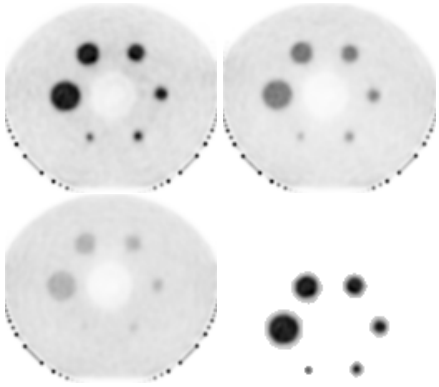

(a) SBR = 8.40:1

(b) SBR = 5.06:1 (c) SBR = 2.59:1

Figure 4: First row: phantom PET images, with three different SBRs. Second row: segmentation results. MIP visualization.

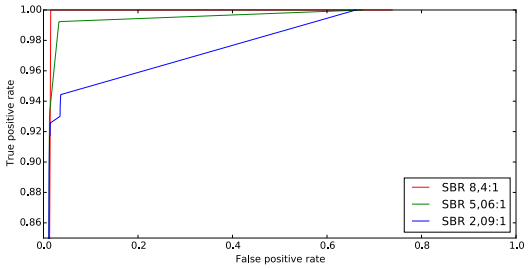

Figure 5: ROC curves for the relative thresholding based on attribute-based approach, for various SBRs (see Figure 4).

A complete procedure combining the shaping detection framework with a standard SUV-based segmentation strategy is available in the Beth Israel Plugin for Fiji software. It works as follows. Considering the detected lesions mask (i.e. the detection framework output), the first step of the segmentation process is to produce automatically a larger region of interest (ROI) encompassing each detected high-intensity region, in order to reproduce the

bounding boxes commonly defined manually in local approaches. To do so, we adopt a region-growing based approach using as seeds/markers the compact high-intensity regions automatically identified with the detection procedure. Each new voxel is added to the ROI if its SUV is closer to the seed intensity (i.e. the mean intensity of all the voxels detected and/or iteratively aggregated to the region) compared to the background (i.e. the mean intensity of the voxels that are not included in the mask). To avoid unlimited growing of low contrast uptake and reduce time / memory consumption, we considered intensity values from a modified SUV-based PET image in which SUV intensities below 2.5 are set to 0 (background). At this stage, a manual correction is possible to remove physiological uptakes and / or add missing regions (with low contrast or which do not fulfill the compacity shape criterion). Then any SUV-based segmentation method can be applied in these automatically defined ROIs to produce final tumour contours, such as 41% SUVmax lesion based threshold (Meignan and et al., 2014), which is currently integrated in Fiji.

6.3.2. Ongoing clinical evaluation

Introduced as a relevant tumour burden quantification on baseline PET and an additional prognostic factor to predict patient outcome (Cheson and et al., 2014; Kanoun and et al., 2014; Cottereau and et al., 2018), the total metabolic tumour volume (TMTV) has never reached clinical application due to the lack of a fast and user-friendly automated determination. In this context, our shaping-based software tool could offer a fast, automatic and reproducible setting for tumours detection and help reduce intra- and inter-user variability for tumour burden assessment. This tool could thus encourage the implementation of TMTV in clinical routine for patients' risk assessment in lymphomas. To this end, a large-scale multi-center clinical study is ongoing, evaluating the variability, accuracy and computation time of TMTV calculation between a standard fully-manual approach and our method.

In particular, in (Cottereau and et al., 2019), our method has been used to demonstrate that the TMTV was a strong predictor of the progressions of the disease and deaths in a prospective series of 301 patients with diffuse large B cell lymphomas. In this study the volume has been computed by two independent observers. In a test set of 25 patients, the Lin concordance correlation coefficient was 0.998 (95% CI 0.997–0.999). The inter-observer agreement on the dichotomization of patients in low and high TMTV groups for survival prediction, based on a TMTV cutoff of 200 cm^3, was excellent with a Cohen's $\kappa = 1$.

7. Conclusion

This article has proposed a methodological scheme for analyzing PET images with the paradigm of shaping, i.e. by computing and processing the component-tree of the component-tree of an image. In this context, we observed that it was possible to embed high-level prior information (here, a compacity attribute; but any other scalar feature may also be considered) whereas preserving the ability to carry out simple, interactive thresholding procedures on the data. In particular, this allows the medical practitioners to effectively act on the method / tool, and easily understand its behaviour.

From a methodological point of view, the perspectives of this work are twofold. First, they can consist of considering no longer one image, but many. Indeed, in the context of nuclear imaging, PET images are generally coupled with X-ray Computed Tomography data. This opens the way to the developement of shaping on hierarchical models designed for multivalued data. In particular, preliminary studies involving component-graphs have been proposed (Grossiord and et al., 2015b, 2019). More generally, many kinds of hierachical models designed to handle multivalued images may also be considered, and involved in shaping approaches. Other perspectives could be to enrich the priors guiding the segmentation. A unique criterion, combining intensity and compacity priors, may not be sufficiently specific and representative for all lymphoma lesions. Therefore, considering machine (Grossiord and et al., 2017) or deep learning procedures on morphological hierarchy models could help rely on relevant image descriptors that capture physiological phenomena more comprehensively.

References

Alvarez Padilla, F.J., et al., 2015. Multicriteria 3D PET image segmentation, in: IPTA, pp. 346–351.

Alvarez Padilla, F.J., et al., 2018a. Hierarchical forest attributes for multimodal tumor segmentation on FDG-PET/contrast-enhanced CT, in: ISBI, pp. 163–167.

Alvarez Padilla, F.J., et al., 2018b. Matching filtering by region-based attributes on hierachical structures for image co-segmentation, in: ICIP, pp. 131–135.

Caldairou, B., Passat, N., Naegel, B., 2010. Attribute-filtering and knowledge extraction for vessel segmentation, in: ISVC, Part I, pp. 13–22.

Carlinet, E., Géraud, T., 2014. A comparative review of component tree computation algorithms. IEEE Transactions on Image Processing 23, 3885–3895.

Cheson, B.D., et al., 2014. Recommendations for initial evaluation, staging, and response assessment of Hodgkin and non-Hodgkin lymphoma: the Lugano classification. Journal of Clinical Oncology 32, 3059.

Cottereau, A., et al., 2019. High total metabolic tumor volume at baseline allows to discriminate for survival patients in response after R-CHOP: An ancillary analysis of the REMARC study. Hematological Oncology 37, 49–50.

Cottereau, A.S., et al., 2018. Prognostic value of baseline metabolic tumor volume in early-stage Hodgkin lymphoma in the standard arm of the H10 trial. Blood 131, 1456–1463.

Dufour, A., Tankyevych, O., Naegel, B., Talbot, H., Ronse, C., Baruthio, J., Dokládal, P., Passat, N., 2013. Filtering and segmentation of 3D angiographic data: Advances based on mathematical morphology. Medical Image Analysis 17, 147–164.

Grossiord, É., et al., 2015a. Hierarchies and shape-space for PET image segmentation, in: ISBI, pp. 1118–1121.

Grossiord, É., et al., 2015b. Shape-based analysis on component-graphs for multivalued image processing, in: ISMM, pp. 446–457.

Grossiord, É., et al., 2017. Automated 3D lymphoma lesion segmentation from PET/CT characteristics, in: ISBI, pp. 174–178.

Grossiord, É., et al., 2019. Shape-based analysis on component-graphs for multivalued image processing. Mathematical Morphology – Theory and Applications 3, 45–70.

Guigues, L., et al., 2006. Scale-sets image analysis. International Journal of Computer Vision 68, 289–317.

Jones, R., 1999. Connected filtering and segmentation using component trees. Computer Vision and Image Understanding 75, 215–228.

Kanoun, S., et al., 2014. Baseline metabolic tumour volume is an independent prognostic factor in Hodgkin lymphoma. European Journal of Nuclear Medicine and Molecular Imaging 41, 1735–1743.

Kanoun, S., et al., 2016. Beth Israel Plugin for FIJI: Logiciel gratuit et open source pour la recherche scientifique. Médecine Nucléaire 40, 194.

Meignan, M., et al., 2014. Metabolic tumour volumes measured at staging in lymphoma: methodological evaluation on phantom experiments and patients. European Journal of Nuclear Medicine and Molecular Imaging 41, 1113–1122.

Salembier, P., et al., 1998. Anti-extensive connected operators for image and sequence processing. IEEE Transactions on Image Processing 7, 555–570.

Salembier, P., Wilkinson, M.H.F., 2009. Connected operators. A review of region-based morphological image processing techniques. IEEE Signal Processing Magazine 26, 136–157.

Urien, H., et al., 2017. Brain lesion detection in 3D PET images using max-trees and a new spatial context criterion, in: ISMM, pp. 455–466.

Wilkinson, M.H.F., Westenberg, M.A., 2001. Shape preserving filament enhancement filtering, in: MICCAI, pp. 770–777.

Xu, Y., et al., 2016. Connected filtering on tree-based shape-spaces. IEEE Transactions on Pattern Analysis and Machine Intelligence 38, 1126–1140.